Left Atrial Appendage Contraction Analysis: A Preliminary Test on Atrial Fibrillation Patients

Sachal Hussain[1], Matteo Falanga[1], Alessandro. Dal Monte[2], Corrado Tomasi[2], Cristiana Corsi[1]

[1] DEI, University of Bologna, Campus of Cesena, Bologna, Italy
[2] Santa Maria delle Croci Hospital, AUSL della Romagna, Ravenna, Italy

Abstract

In atrial fibrillation (AF), about 80% of the thrombi originates in left atrial appendage (LAA). However, it is still unclear how and to what extent LAA impaired mechanical contraction and the consequent compromised blood wash-out affects thrombogenesis. In this study, we proposed a novel approach to extract the centerline of LAA and defined different contraction parameters to assess the global impact of AF on LAA. Moreover, we also sub-divided the LAA into different regions and then performed regional contraction analysis. Up to now, we have tested this approach on patient-specific dynamic models of LAA, acquired from 5 normal subjects and 5 AF patients. Our algorithm successfully defined the LAA centerline, irrespective of the existence of variable LAA morphologies and with the help of global and regional contraction parameters, the differences in the contractility of LAA in normal and AF patients were demonstrated.

1. Introduction

The left atrial appendage (LAA) is a complicated tubular structure possessing a narrow orifice that connects it to the left atrium body [1,2]. Furthermore, it carries unique anatomical and physiological properties [3]. In the past it was considered a relatively insignificant structure of cardiac anatomy; more recently, with continued in-depth analysis, the LAA is now considered a predominant location for thrombus development in individuals afflicted with non-valvular atrial fibrillation (AF) [4]. In fact, approximately 90% of the thrombus in AF occurs within the LAA [5]. Patients affected by AF exhibit improper contractility of the LAA, leading to stagnant blood flow within the LAA and increasing the risk of thrombus blood flow, ultimately resulting in stroke [6]8].

Moreover, the in-depth analysis of the contraction of LAA is still missing. Therefore, in this study, we aim to assess the contractility of LAA and to evaluate the differences in contraction between normal and pathological LAA anatomies. For this purpose, we are proposing a novel approach of extracting the centerline of LAA and with reference to the centerline, we are defining LAA global contraction parameters. In addition, we are dividing LAA into distinct regions and evaluating regional LAA contraction parameters.

2. Material and Methods

2.1. Dynamic image data acquisition

CT dynamic acquisitions of the heart were obtained for five patients with AF with a control (CTRL) group of five normal subjects having normal size of heart structures and no previous history of AF.

Volumetric CT images were reconstructed for a total of 10 phases from ventricular end diastole. Each reconstructed CT volume was 512x512x200 pixels. The voxel resolution was not isotropic: in-plane resolution was 0.39 mm, and through-plane resolution was 1 mm, resulting in a voxel size of $0.39 \times 0.39 \times 1$ mm^3.

2.2. Image segmentation

To reconstruct surfaces, the first acquired volume along cardiac cycle was considered. An active contour algorithm was used, which was previously developed in MATLAB environment. For segmentation, an algorithm based on deformable model theory was restricted to LA chamber including LAA only, by defining a region of interest (ROI), and then initialized. Evolution was stopped when

deformable surface meets the LA endocardium. The resulted surface in stereolithography format.

In the next step, an affine transformation was applied between ten CT volumes of each dataset. The rigid LA motion was subsequently enhanced by employing a 3D non-rigid registration technique that is founded on the B-spline transformation model [9], utilizing the mean square difference as a measure of similarity. Following the registration procedure, the displacements between frames were implemented on the vertices of the LA surface to reconstruct the LA surfaces along the cardiac cycle [10].

2.3. Post processing of surfaces

Before applying the centreline extraction approach, Laplacian smoothing was implemented on the LA surfaces.

Then the LA appendage, specifically at its orifice, was manually detached from the LA body based on visual observation, taking into consideration the surface's curvature, and incorporating the ridge within the LA chamber (Figure 1a).

2.4. LAA centerline extraction and regionalization

As a first step of LAA centerline extraction method, the best fitting LAA orifice plane was computed (Figure 1(a)). Then this plane was translated in the orthogonal direction to the orifice plane, towards the tip of LAA. As the translated plane intersected the LAA surface, the intersecting points were considered to compute the new barycenter. Using this barycenter and the intersecting points, a new best fitting plane was formulated, having the normal in the direction of previous barycenter and the new barycenter (Figure 1(b)). Then, if the new plane completely intersects the LAA, then the intersection was considered correct and complete. In case of incomplete intersection, a rotation was applied to the plane till the intersection was completed (Figure 1c). Using these intersecting points, the barycenter was computed and considered as one of the points of the centerline of LAA. These steps were repeated till the tip of the LAA was reached and by connecting all the points, LAA centerline was generated (Figure 1d).

After the extraction of LAA centerline, LAA regionalization was applied to explore regional differences. For this step, the LAA surface was partitioned into three regions by splitting LAA

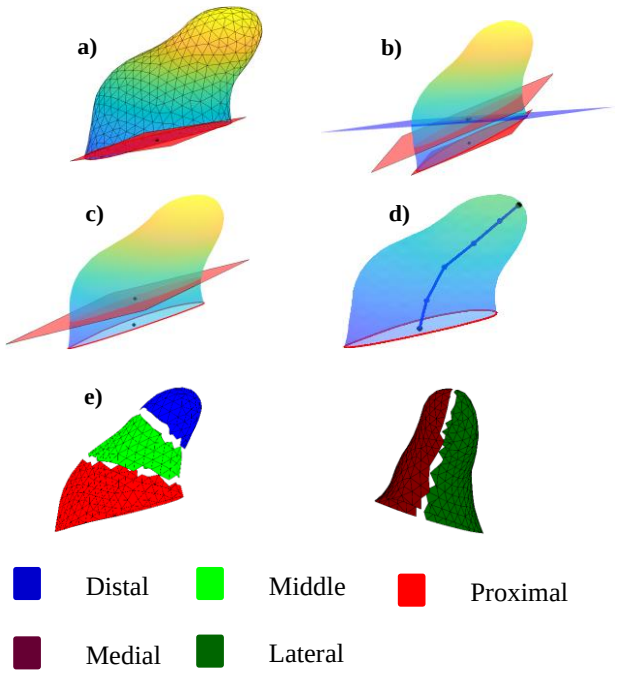

Figure 1: a) LAA surface with best fitting ostium plane (red) and barycenter of ostium (black dot). b) LAA surface with translated ostium plane (red) and newly generated intersecting plane (blue). c) LAA surface with newly generated rotated intersecting plane along with the barycenter of the ostium and the intersecting points (black dots). d) LAA surface with piecewise linear centerline, starting from the ostium barycenter till the tip of the LAA surface. e) (left) subdivision of LAA into 03 regions, (right) subdivision of LAA into 02 regions.

centerline into equidistant sections. These regions were named proximal, medial, and distal from the LAA to the tip (Figure 1e, left). Subsequently, LAA was divided into two regions along its longitudinal direction, using the centerline best fitting plane. In this step, the region towards the LA body was identified as the medial region while the region towards the mitral annulus was labeled as the lateral region (figure 1e, right).

To justify that the proposed LAA centerline extraction approach has the capability to work on variable LAA morphologies. This algorithm was tested on the four classical structural morphologies of LAA, presented in the literature [12]. The classification system was based on the shape and structure of LAA and identified them as: “Chicken wing” being the most common (48%), followed by “Cactus” (30%), “Windsock” (19%), and “Cauliflower” being the least common (3%) [13].

2.5. LAA contraction parameters

Standard primary parameters throughout the cardiac cycle were computed to assess LAA function including LAA volume-time curve, LAA ejection fraction (EF), LAA orifice area, LAA centerline length and tortuosity.

To assess regional changes, region-based contraction parameters were defined. For each region, regional radial dimension (RRD) was evaluated, as the average of Euclidean distance of each vertex belonging to a specific region from the centerline; regional radial strain (RRS) was then computed as:

$$\mathrm{RRS}(x) = \frac{\mathrm{RRD}(x) - \mathrm{RRD}_{\min}}{\mathrm{RRD}_{\min}} \cdot 100$$

where RRD(x) is the current regional radial dimension at the time x and $\mathrm{RRD}_{\min}$ is the minimum regional radial dimension throughout the cardiac cycle. Once RRS was computed for each region, the global radial strain (RS) was calculated as the average RRS value of medial and lateral at each frame. To compute longitudinal strain, the variation in the length of LAA centerline was traced out throughout the cardiac cycle with reference to the minimum of LAA centerline length, using this formula:

$$\mathrm{LS}(x) = \frac{\mathrm{LAA}_{\mathrm{len}}(x) - \mathrm{LAA}_{\mathrm{len\_min}}}{\mathrm{LA}_{\mathrm{len\_min}}} \cdot 100$$

where $\mathrm{LA}_{\mathrm{len}}(x)$ is the LAA centerline length at current frame x and $\mathrm{LA}_{\mathrm{len\_min}}$ is the minimum LAA centerline length throughout the cardiac cycle.

Contraction of each region was assessed in terms of regional wall motion (RWM), calculated as the difference between current RRD and minimum RRD for each region.

The index of LAA asynchrony ($\mathrm{IA}_{\mathrm{RWM}}$) was computed separately among the three regions and the two regions. Finally, for each surface region, regional peak wall motion was divided by peak regional radial dimension to obtain regional shortening fraction (RSF). RSF was computed for each surface segment and averaged for each subject.

3. Results and Discussion

Anatomical models derived from CT imaging were analysed in 5 normal subjects and 5 AF patients. The approach was found feasible in all subjects.

Centerline detection in all the four different morphologies of the LAA was successful. In Figure 2 we show an example for each LAA type.

LAA orifice area, RRS and RSF for proximal region demonstrated statistically significant differences ($p<0.05$) between the two groups. However, in this small study, other parameters like global longitudinal strain, global radial strain and $\mathrm{IA}_{\mathrm{RWM}}$ did not report significant differences. The main findings have been reported in Figure 3.

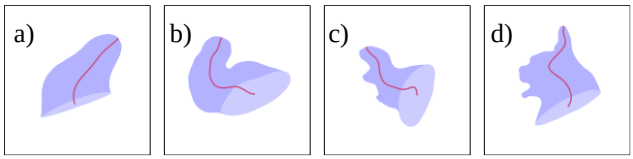

Figure 2: Centerline extraction of variable morphological anatomies of LAA. a) Windsock. b) Chicken wing. c) Cactus. d) Cauliflower.

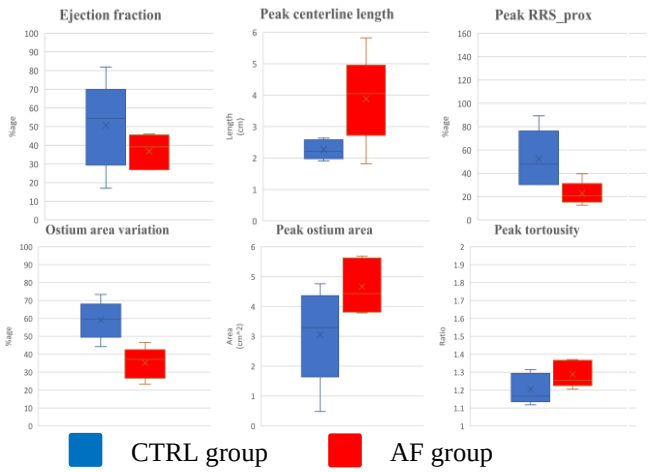

Figure 3: Computed LAA contraction parameters in CTRL and AF group

Among all the parameters, LAA orifice area variation presented statistically significant differences. The median LAA orifice area percentage variation in CTRL group was 59.6% in comparison with 37.1% in AF group ($p < 0.005$) which potentially highlights the disturbed contractility in AF group. It was also seen that the LAA centerline length, LAA orifice area and LAA tortuosity values were higher in the AF group compared to CTRL which showed the existence of dilation and complex morphological behavior of LAAs in AF group. Nevertheless, the differences were found to be not statistically significant.

For region-based analysis, the LAA was subdivided into distinct regions. Nonetheless, only the proximal region showed the significant differences between CTRL and AF groups in terms of RRS and RSF. For proximal region, mean peak RRS in CTRL group was 47.9% while in AF group, it was 20.7% ($p = 0.05$). Similarly, mean peak RSF in the CTRL group was 0.32 and 0.17 in the AF group ($p <0.05$). This assessment strengthens the previous result where dysfunctionality in the contraction of LAA orifice was detected as the orifice is a part of proximal region.

The proposed approach has several limitations, and this is because of the complex, curvy shape of LAA and the

existence of high variability in the morphology of the LAA. In some cases, when there exist multiple lobes, the identification of primary lobe can be misleading which generates incorrect centerline and ultimately includes error in the quantification of contractility. In such cases, there is a possibility to manually identify the main lobe and re-generate the centerline, which makes this method semiautomatic.

4. Conclusion

To conclude, the approach presented in this study has the potential to extract the centerline of LAA irrespective of the morphological variations in LAA. Furthermore, the proposed LAA contraction parameters have the capability to assess and quantify the global and regional contractility of LAA.

Acknowledgments.

This work was supported by PersonalizeAF project. This project has received funding from the European Union's Horizon 2020 research and innovation program under the Marie Skłodowska-Curie grant agreement No 860974.

References

[1] N. M. Al-Saady, O. A. Obel, and A. J. Camm, "Left atrial appendage: Structure, function, and role in thromboembolism," *Heart*, vol. 82, no. 5, pp. 547–554, 1999, doi: 10.1136/hrt.82.5.547.

[2] S. Saygi, "Atrial fibrillation and the role of LAA in pathophysiology and clinical outcomes?," *J. Atr. Fibrillation*, vol. 5, no. 3, pp. 153–160, 2012.

[3] W. Aschenberg, M. Schlüter, P. Kremer, E. Schröder, V. Siglow, and W. Bleifeld, "Transesophageal two-dimensional echocardiography for the detection of left atrial appendage thrombus," *J. Am. Coll. Cardiol.*, vol. 7, no. 1, pp. 163–166, 1986, doi: 10.1016/S0735-1097(86)80275-3.

[4] J. L. Blackshear, J. A. Odell, and F. Ed, "Appendage Obliteration to Reduce Stroke in Cardiac Surgical Patients With Atrial Fibrillation," 1996.

[5] W. D. Johnson, A. K. Ganjoo, C. D. Stone, R. C. Srivyas, and M. Howard, "The left atrial appendage: Our most lethal human attachment! Surgical implications," *Eur. J. Cardio-thoracic Surg.*, vol. 17, no. 6, pp. 718–722, 2000, doi: 10.1016/S1010-7940(00)00419-X.

[6] A. Masci, L. Barone, L. Dedè, M. Fedele, C. Tomasi, and C. P. Bradley, "The Impact of Left Atrium Appendage Morphology on Stroke Risk Assessment in Atrial Fibrillation : A Computational Fluid Dynamics Study," vol. 9, no. January, pp. 1–11, 2019, doi: 10.3389/fphys.2018.01938.

[7] R. Beigel, N. C. Wunderlich, S. Y. Ho, R. Arsanjani, and R. J. Siegel, "The left atrial appendage: Anatomy, function, and noninvasive evaluation," *JACC Cardiovasc. Imaging*, vol. 7, no. 12, pp. 1251–1265, 2014, doi: 10.1016/j.jcmg.2014.08.009.

[8] L. Di Biase *et al.*, "Stroke Risk in Patients With Atrial Fibrillation Undergoing Electrical Isolation of the Left Atrial Appendage," *J. Am. Coll. Cardiol.*, vol. 74, no. 8, pp. 1019–1028, 2019, doi: 10.1016/j.jacc.2019.06.045.

[9] M. Unser, "Splines: A perfect fit for signal and image processing," *IEEE Signal Process. Mag.*, vol. 16(6), no. NOVEMBER, pp. 22–38, 1999.

[10] A. Masci *et al.*, "A Proof of concept for computational fluid dynamic analysis of the left atrium in atrial fibrillation on a patient-specific basis," *J. Biomech. Eng.*, vol. 142, no. 1, pp. 1–11, 2020, doi: 10.1115/1.4044583.

[11] Autodesk Meshmixer, "Meshmixer 3.5," 2018. http://www.meshmixer.com

[12] Y. Wang, L. Di Biase, R. P. Horton, T. Nguyen, P. Morhanty, and A. Natale, "Left atrial appendage studied by computed tomography to help planning for appendage closure device placement," *J. Cardiovasc. Electrophysiol.*, vol. 21, no. 9, pp. 973–982, 2010, doi: 10.1111/j.1540-8167.2010.01814.x.

[13] L. Di Biase *et al.*, "Does the left atrial appendage morphology correlate with the risk of stroke in patients with atrial fibrillation? Results from a multicenter study," *J. Am. Coll. Cardiol.*, vol. 60, no. 6, pp. 531–538, 2012, doi: 10.1016/j.jacc.2012.04.032.

Address for correspondence:
Sachal Hussain
DEI, University of Bologna,
Via dell'Università 50, 47522 Cesena (FC), Italy
sachal.hussain3@unibo.it